Construction and Building Materials 367 (2023) 130361

Contents lists available at ScienceDirect

Construction and Building Materials

journal homepage: www.elsevier.com/locate/conbuildmat

Influence of calcination temperature on hydration behavior, strength, and weathering resistance of traditional gypsum plaster

Kerstin Elert *, Pedro Bel-Anzué, Miguel Burgos-Ruiz

Granada University, Department of Mineralogy and Petrology, Fuentenueva S/N, 18071 Granada, Spain

ARTICLE INFO

Keywords:
Bassanite
Anhydrite
Surface hardness, Compressive strength
Flexural strength
Weathering

ABSTRACT

The mineralogical composition, microstructure, and reactivity of traditional gypsum, a multiphase product, is closely connected to its calcination temperature, but systematic studies which relate those features to mechanical properties and weathering resistance of plasters are scarce. Here we examined the hydration behavior of gypsum calcined between 100 and 1000 °C, which contained varying amounts of uncalcined gypsum, bassanite, and/or anhydrite II.

Detailed hydration and textural studies allowed the identification of the underlying mechanisms leading to differences in plaster performance related to (i) delayed hydration of anhydrite II along with modifications of the pore system; (ii) a filler effect exerted by anhydrite II and uncalcined gypsum; (iii) disruption of the plaster matrix by uncalcined gypsum; (iv) seeded crystallization in the presence of uncalcined gypsum and anhydrite II. Findings of this study further the understanding of traditional gypsum plaster performance and open opportunities for the development of sustainable building materials by designing optimized gypsum-based mixtures for specific application.

1. Introduction

Gypsum ($CaSO_4{\cdot}2H_2O$) has been an important building material since ancient times and was traditionally used for a wide variety of interior/exterior and structural applications (Fig. 1), including columns, load-bearing walls, arches, vaults, cantilevered staircases, façades, and floors [1–3]. By comparison, todaýs industrially produced gypsum is essentially limited to interior use for finishing and decorative purposes [4]. The proximity of large gypsum deposits was certainly a decisive factor for extensive gypsum use in monumental and popular architecture in many regions [3,5]. However, it has also been suggested that the widespread, more versatile use of traditional gypsum originated from its superior mechanical strength and weathering resistance as compared to modern gypsum-based materials. The former was typically calcined at higher temperatures, which led to a multiphase product. Depending on the calcination *T* this product might contain bassanite ($CaSO_4{\cdot}0.5H_2O$) and anhydrite ($CaSO_4$) together with small quantities of uncalcined gypsum, (activated) clay minerals, quartz, carbonates, and (at high *T*) quicklime [6]. Modern building gypsum obtained under controlled calcination conditions at low temperature (i.e., 135–180 °C), in contrast, is generally of high purity and contains mainly bassanite, (β-hemihydrate [7]).

Experimental calcination has shown that *T* of up to ~ 1000 °C can be reached in traditional gypsum kilns [2,8,9] and numerous analyses of historic gypsum mortars and plasters from various European countries (e.g., Portugal, Italy, Poland, and Germany) have revealed the presence of significant amounts of anhydrite [4,10,11,12]. Considering that *T* in traditional kilns was not homogeneous and that the highest *T* was only reached close to the combustion chamber [2], gypsum stones underwent different degrees of calcination depending on their location within the kiln. Furthermore, calcination might have been incomplete in the case of large gypsum stones (Fig. 2a) and the core of these stones could still contain uncalcined gypsum. Uncalcined gypsum was usually removed prior to further processing as it complicated manual grinding due to its elevated hardness, while the remaining calcined gypsum was commonly ground without any further sorting [2] to obtain a multiphase product with commonly high anhydrite II content [9].

Research related to traditional multiphase gypsum has mainly focused on the mineralogical and textural characterization of historic mortars and plasters [6,10,11,12,13]. There is, however, a lack of systematic studies which correlate the properties of the set plaster (i.e., mechanical strength and weathering resistance) with the calcination

* Corresponding author.
E-mail address: kelert@ugr.es (K. Elert).

https://doi.org/10.1016/j.conbuildmat.2023.130361
Received 31 August 2022; Received in revised form 3 January 2023; Accepted 8 January 2023
Available online 12 January 2023

conditions of the raw material and its hydration behavior. Most recent investigations focus on waste by-product/recycled gypsum-based materials (e.g., phosphogypsum [14], flue gas desulfurization gypsum [15], or recycled building waste gypsum [16]), which are normally calcined at $T < 200$ °C to obtain sustainable building materials [14–18]. Studies involving higher calcination T typically use by-product gypsum (i.e., phosphorgypsum with and without additives) and the resulting mineralogical composition and hydration behavior are not comparable with those of traditional gypsum [19,20]. In order to fill the existing knowledge gap regarding the influence of calcination T on the performance of historic multiphase plaster, raw gypsum was calcined over a wide T range (100–1000 °C) in order to mimic the traditional calcination process and obtain material representative of calcined gypsum stones from different locations within the kiln. Hydration of the calcined product was performed in small batches to determine its reactivity (hydration kinetics) as well as the mechanical strength and weathering resistance of the cured plaster. Test results are discussed considering mineralogical and textural features of the calcined and hydrated gypsum obtained at different T in order to explain the underlying mechanisms controlling the performance of traditional multiphase gypsum.

The outcome of this investigation not only provides important insight into the effect of the traditional calcination process on the performance of gypsum plaster, but will also help practitioners to formulate compatible multiphase products for specific applications in the field of heritage conservation and new constructions. The latter is of special importance as gypsum has the potential of replacing building materials with greater carbon footprint and could contribute to the sustainability of modern constructions [7]. Indeed, gypsum does not release CO_2 upon calcination and requires lower calcination T as compared to other binders such as lime (~900 °C) or Portland cement (~1400 °C), thus reducing production costs and environmental impact. Furthermore, its grinding is less energy intensive as compared to clinker grinding in the case of Portland cement, and gypsum-based construction waste might easily be recycled by simple calcination, thus contributing to a circular economy [21].

2. Materials and methods

2.1. 1. Materials and sample preparation

Gypsum from outcrops close to the village of Calamocha (Teruel, Spain), a region which has a long tradition of architectural gypsum use, was extracted manually [2] and separated into small pieces of approximately 1.5 cm x3 cm x4 cm. Note that this type of gypsum has traditionally been used for exterior rendering [8]. Calcination was performed in an electric furnace (Model CR-35, Herotec, Spain) over a wide T range from 100 to 1000 °C at a heating rate of ~ 1.8 °C/min (Fig. 2b) in order to mimic the firing process in traditional gypsum kilns based on *in situ* T measurements during a traditional field calcination using firewood [2]. Small batches were extracted from the furnace at predetermined temperatures (i.e., 100, 150, 200, 250, 300, 350, 400, 500, 600, 700, 800, 900, and 1000 °C) for analysis and plaster preparation.

About 50 g of gypsum calcined at each target T were ground manually and mixed with MilliQ® water (water/solid ratio = 0.6). Cylindrical (2.5 cm in diameter and 0.5 cm height, used for weathering tests) and prismatic plaster samples (1 cm x 1 cm x 4 cm, used for all other tests) were prepared using flexible rubber or plasticine molds, respectively. Plaster samples were demolded after 1 day and cured under laboratory conditions (i.e., 20 ± 3 °C and 50 ± 5 % RH) for 7 days prior to analysis and testing. It was not possible, however, to obtain coherent plaster samples using gypsum calcined at ≤ 150 °C and ≥ 500 °C as those disintegrated upon demolding. Consequently, these samples were only analyzed with XRD and SEM but could not be subjected to porosity measurements or mechanical and weathering tests.

2.2. Analytical methods and testing

X-ray diffraction (XRD, X'Pert PRO, Malvern Panalytical ltd., UK) was used to determine the mineralogical composition of gypsum before and after calcination, as well as of gypsum pastes upon hydration (using one powder specimen per gypsum sample). Equipment settings: Cu-Kα radiation (λ = 1.5404 Å); Ni filter; 45 kV voltage; 40 mA intensity; exploration range of 3 to 60 °2θ and goniometer speed of 0.05 °2θ/s. Mineral phase identification/quantification using reference intensity ratio (RIR) values, as well as the determination of the crystallite size (applying the Scherrer equation) were performed using XPowder

Fig. 1. Ayyup Castle (Aragon, Spain) built in the 9th century using gypsum blocks and mortar.

software [22]. To determine the hydration kinetics of gypsum pastes using *in situ* XRD, small batches (i.e., 3 g gypsum mixed with MilliQ® water at a 1:1 water/solid ratio) were prepared. Immediately, after mixing, approximately 1 g of paste was filled into powder sample holders and analyzed by XRD. Patterns were collected continuously over a 2.6-hour period and an exploration range of 10–45 °2θ, amounting to a total of 30 successive patterns of 5.17 min duration each. The remaining sample was kept in well-sealed Falcon tubes (together with moist cotton wool to prevent premature drying) and analyzed over a period of up to 5 weeks. In addition, the effect of small amounts of uncalcined gypsum or insoluble anhydrite II calcined at 800 °C (i.e., 1, 5, 10, and 20 wt%) on the hydration of pure bassanite (obtained by calcining gypsum at 200 °C for 6 h) was studied using pastes with a 1:1 water/solid ratio. Samples were analyzed by *in situ* XRD over a ~ 2.6-hour period as described above. Here only gypsum, bassanite (β-hemihydrate) and sparingly soluble/insoluble anhydrite II were considered to determine the composition of calcined gypsum and its hydration evolution. A differentiation between bassanite and readily soluble anhydrite III was not attempted due to the difficulty of assigning individual Bragg peaks to each phase based on conventional XRD analysis, especially since rehydration of anhydrite III to bassanite is a very rapid process and difficult to avoid during sample handling (i.e., grinding) under ambient conditions [23]. Using Raman spectroscopy, Schmid et al. [24] observed complete transformation of anhydrite III into bassanite within 30 min at 80 °C in (humid) air. Even though the presence of anhydrite III cannot be ruled out completely, it seems unlikely that it would have influenced the hydration behavior of the calcined gypsum studied here.

Simultaneous thermogravimetry and differential scanning calorimetry (TG-DSC, Mettler-Toledo TGA/DSC1, Switzerland) were employed to study the dehydration of the original uncalcined gypsum (using one specimen) over a temperature range of 25–450 °C at a heating rate of 10 °C/min in flowing air (100 mL/min).

Textural and compositional characteristics of one carbon-coated specimen per gypsum sample before and after calcination, as well as subsequent hydration were studied using field emission scanning electron microscopy (FESEM, AURIGA, Carl Zeiss, Germany) coupled with energy dispersive spectrometry (EDS, INCA-200, Oxford Instruments, UK). Equipment settings: 10^{-6} Pa vacuum and 3 kV acceleration voltage in secondary electron imaging mode.

Porosity and pore size distribution of cured gypsum plasters (using one specimen per gypsum sample) were determined with mercury intrusion porosimetry (MIP) using an Autopore III 9410 porosimeter (Micromeritics, US). This instrument measures pores with 0.003–360 μm diameter. Samples (0.95 ± 0.11 g) were kept in a dry environment using silica gel for at least 48 h prior to analysis and not oven-dried in order to avoid *T*-induced phase changes [25].

An Instron 3345 (Instron Co., US) was used to determine flexural and compressive strength of cured gypsum plasters using prismatic samples prepared with 0.6 water/solid ratio. Measurements were performed using an adapted version of the procedure described in EN 1015–11 [26], applying a load of 500 N at 6 mm/min. Samples were dried in a ventilated oven for 48 h at 30 °C prior to testing. Again, such low *T* was chosen to avoid *T*-induced phase changes. Reported results are based on at least 3 specimens per plaster sample.

The surface hardness (Leeb hardness, HLD) of cured gypsum plasters was measured using a durometer (rebound hammer, PCE-2500 N, PCE Instruments, Germany). Reported values are based on at least 8 measurements performed on two specimens per plaster sample. In order to obtain additional insights into the effect of gypsum/anhydrite additions on the final surface hardness, a second set of plaster samples with 0.6 water/solid ratio containing (i) 100 wt% bassanite; (ii) 50 wt% bassanite and 50 wt% gypsum; or (iii) 50 wt% bassanite and 50 wt% anhydrite was tested.

Plaster samples were subjected to a non-standard accelerated weathering test in order to determine their resistance to the impact of water spraying and repeated wetting–drying. Cylindrical samples were placed on a vertical metal grid and sprayed on their circular face with deionized water (300 mL/sample·day) at a distance of 20 cm. The circular face was placed in a vertical position so that the water could run off to simulate the effect of rain on a building façade. Spraying was repeated 15 times over a 3-week period. Samples were dried at 30 °C for 24 h in a ventilated oven between tests (i.e., until a constant weight was reached) in order to determine weight loss. Weight loss was calculated considering phase change-related weight gain during testing (i.e., the weight gain due to the hydration of calcium sulfate phases was calculated based on quantitative XRD analysis before and after the spraying test and added to the total weight loss determined for each sample at the end of the test). Tests were performed in duplicate.

3. Results and discussion

3.1. Gypsum calcination

XRD analysis (Fig. 3a) revealed that the uncalcined gypsum was of high purity and complied with European standard EN 13279–1 [27] as it only contained small amounts (≤ 3 wt%) of quartz and carbonates (calcite and/or dolomite), as well as trace amounts of clay (note that quartz, carbonates and clays are not included in Fig. 3). Under the conditions of this laboratory study, which mimic the calcination process in traditional kilns, temperatures ≤ 150 °C did not promote significant dehydration of gypsum and the bassanite content remained below 5 wt %, while anhydrite II was not detected. At 200 °C, in contrast, the main phase was bassanite (~ 80 wt% and ~ 5 wt% anhydrite II) and the gypsum content decreased to ~ 10 wt%. These findings are consistent with TG-DSC data (Fig. S1), showing a split endothermic band corresponding to bassanite and anhydrite III formation at 150 and 165 °C, respectively [28]. Dehydration advanced at 250 °C and gypsum was now only observed in trace amounts (< 1 wt%) together with ~ 5 wt%

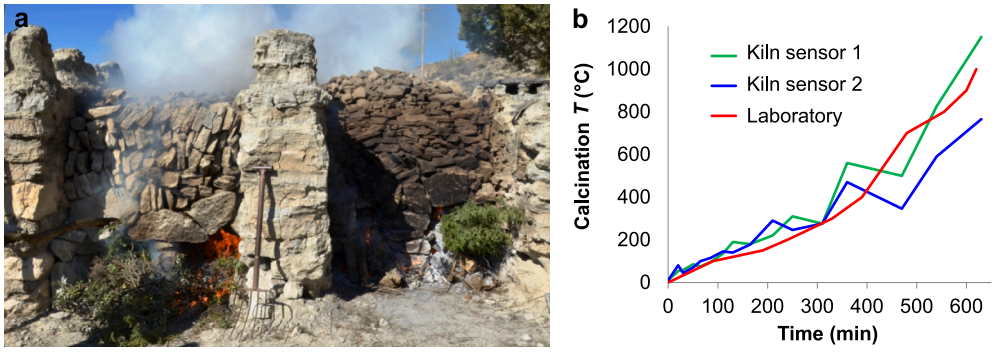

Fig. 2. Traditional calcination: a) field calcination in traditional kilns using gypsum stones of variable size; and b) temperature evolution versus time in an electric furnace (red line), mimicking the calcination process in a traditional kiln (green and blue lines) using firewood [2].

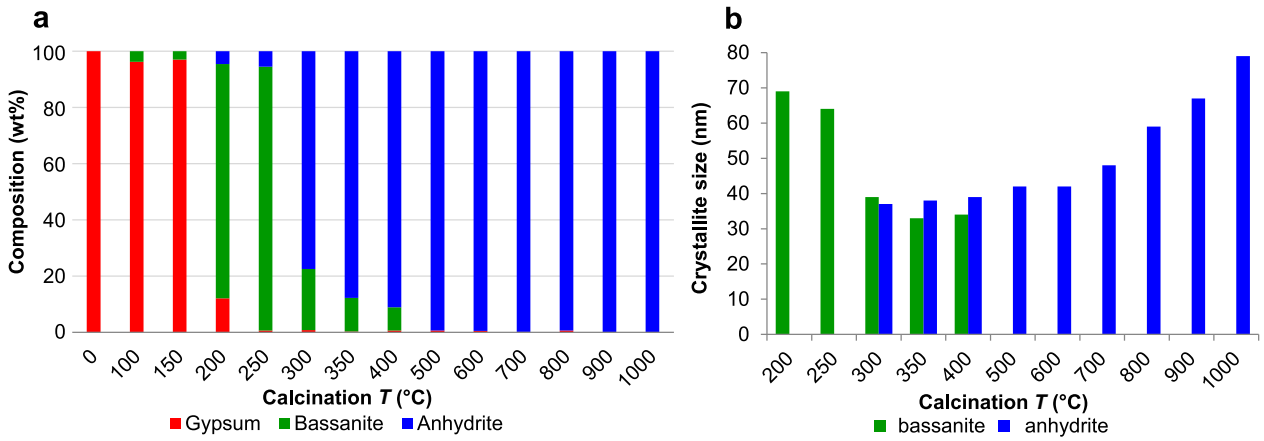

Fig. 3. Calcined gypsum: a) mineralogical composition (wt%) based on XRD analysis and b) crystallite size (nm) of bassanite (200 Bragg reflection) and anhydrite II (020 Bragg reflection) versus calcination *T*.

anhydrite II, while bassanite amounted to ~ 95 wt%. Further *T* rise resulted in a sharp increase in anhydrite II content to ~ 75 wt% at 300 °C and > 95 wt% at 500 °C. The latter findings are in general agreement with TG-DSC data (Fig. S1), revealing an exothermic band centered at 358 °C associated with the transition of soluble anhydrite III to insoluble anhydrite II [28,29].

Measurements of the crystallite size using high-intensity 200 and 020 Bragg peaks of bassanite and anhydrite II, respectively, gave important information on the microstructural evolution upon calcination (Fig. 3b). In the case of bassanite an initially small decrease in crystallite size (< 10 %) at 250 °C was observed, which became more important (> 40 %) at 300–400 °C. The observed reduction in crystallinity was likely due to defect creation associated with incipient dehydration. A similar phenomenon has been reported for other hydrated phases such as $Ca(OH)_2$, where initial water loss resulted in defect creation and a reduction in crystallinity prior to the formation of the dehydrated product (CaO) [30]. Alternatively, the crystallinity reduction could also be related with the formation of anhydrite III, which has been reported for a temperature range between ~ 170–460 °C [31], but cannot be unambiguously identified with conventional XRD. Anhydrite II suffered a continuous crystallite size increase upon calcination, which was initially negligible (i.e., between 300 and 600 °C) but became more pronounced at $T \geq 700$ °C. An identical trend was observed by Dariz et al. [32] who detected a concomitant reduction in specific surface area at $T > 600$ °C. These changes are characteristic of sintering processes [33] and explain the observed decrease in anhydrite reactivity with increasing calcination *T* (see section 3.2.).

FESEM images provided detailed information on textural changes upon calcination. Uncalcined gypsum (Fig. 4a) showed the typical plate-like morphology with overdeveloped (0 1 0) faces, having the lowest surface energy and corresponding to the primary cleavage plane of gypsum [34]. Cleavage is favored along the {010} planes due to the presence of layers of water molecules, which alternate with layers of calcium and sulfate ions [35]. During the calcination of gypsum, phase transitions occur that follow a topotactic mechanism [36]. This means that the reactant acts as a template and a clear structural relationship

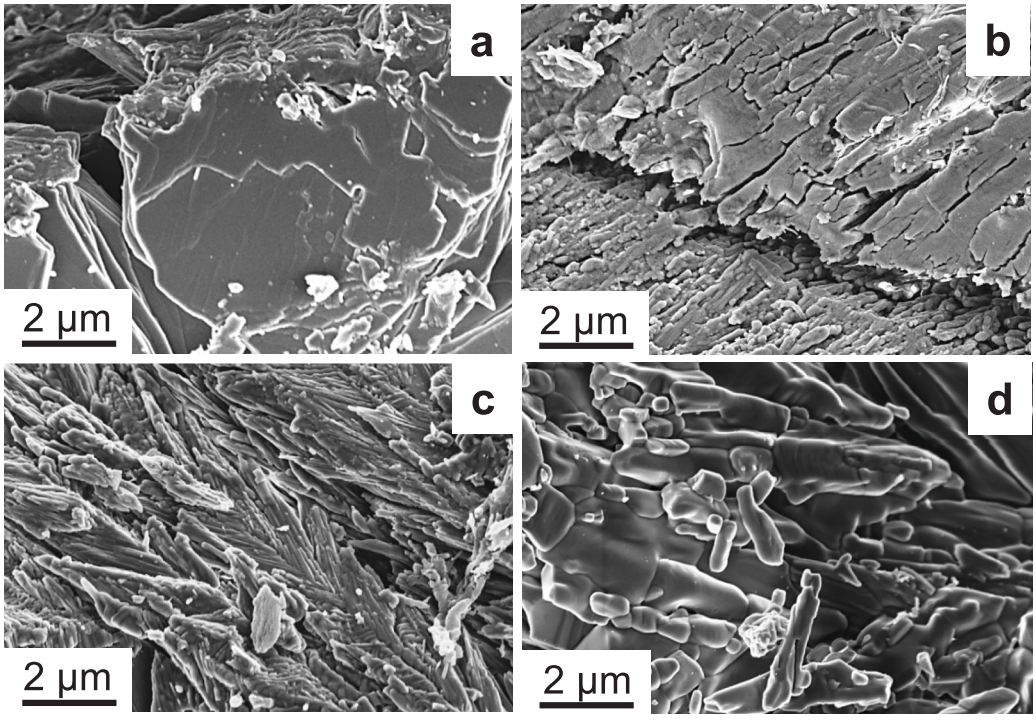

Fig. 4. FESEM images of gypsum: a) uncalcined gypsum showing delamination along primary {0 1 0} cleavage planes; b) gypsum calcined at 200 °C containing > 80 wt% bassanite (note the extensive cracking associated with shrinkage along specific [*hkl*] directions due to H_2O loss); c) gypsum calcined at 400 °C containing ~ 90 wt% anhydrite (note the feather-like morphology); and d) gypsum calcined at 800 °C showing larger anhydrite grains with smooth surfaces and rounded edges due to sintering.

between parent and product phases exists [37]. At 200 °C the formation of abundant microfractures was observed, which was caused by volume changes upon calcination (Fig. 4b). According to Pritzel et al. [29], thermal decomposition of gypsum is initially accompanied by an expansion, which, however, is followed by a contraction once bassanite starts forming, thus resulting in crack development. The latter is not surprising, considering that the molar volume of gypsum (74.23 cm^3/mol) and bassanite (53.21 cm^3/mol) differs by almost 30 %. The formation of bassanite is accompanied by a rearrangement of water molecules, which now form water channels instead of planes [35]. Gypsum calcined at 400 °C (Fig. 4c) contained ~ 90 wt% anhydrite and exhibited a feather-like morphology likely due to further mineral contraction, which can be explained by the additional reduction in molar volume of ~ 15 % upon formation of anhydrite II (45.64 cm^3/mol molar volume). At 800 °C (Fig. 4d) the anhydrite morphology changed significantly, and grains now showed a smooth surface and rounded edges due to sintering. Apparently, smaller anhydrite grains were fused into neighboring bigger ones via surface diffusion, following an Ostwald ripening mechanism, which led to an increase in size [38].

3.2. Gypsum hydration

As expected, bassanite and the small amount of anhydrite in gypsum calcined at ≤ 250 °C hydrated readily and transformed almost completely into gypsum through a dissolution/precipitation process (Fig. 5a) [37]. It was observed that differences in the 020/$\overline{1}$ 21 Bragg peak intensity ratio can be used to distinguish between uncalcined gypsum (having a peak ratio of 3.1–7.2) and gypsum formed upon hydration (having a peak ratio of 1.0–1.1, Fig. S2). The reduction in peak ratio is consistent with the reduction in the relative surface area of the (0 1 0) faces due to the change in crystal habit from plate-like in uncalcined gypsum to acicular crystals in gypsum formed upon hydration (see FESEM results below).

Higher calcination *T* rendered anhydrite less reactive, and a large portion did not hydrate in plasters with a 0.6 water/solid ratio cured at 20 ± 3 °C and 50 ± 5 % RH for 7 days. Indeed, < 50, 25, and 10 % of anhydrite hydrated and transformed into gypsum in plasters prepared with gypsum calcined at 300, 400, and 500 °C, respectively (Fig. 5a). Considering that the water/solid ratio of historic gypsum might have been as low as 0.4 [4], incomplete hydration is probable and is consistent with large amounts of anhydrite detected in ancient plasters and mortars [4,10,11,12].

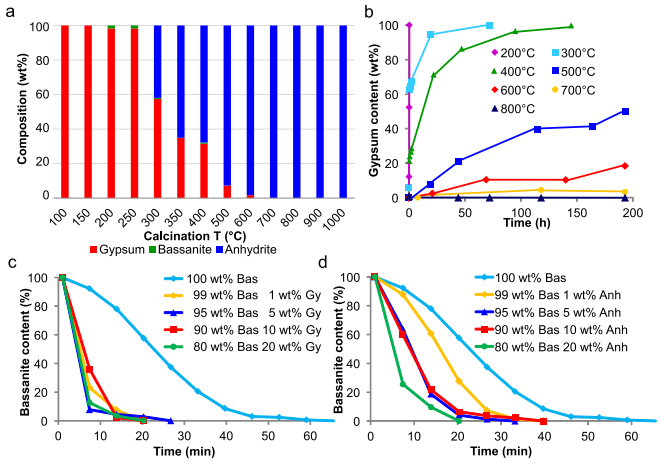

Fig. 5. Hydration of calcined gypsum based on XRD analysis: a) mineralogical composition (wt%) of gypsum plasters with 0.6 water/solid ratio after 7-day curing; b) evolution of the gypsum content (wt%) upon prolonged hydration of gypsum pastes with a 1:1 water/solid ratio; and hydration of bassanite with c) gypsum and d) anhydrite II additions (seeded crystallization). Bas = bassanite, Gy = gypsum, and Anh = anhydrite (lines in (b-d) are a guide to the eye).

The *in situ* XRD study of the hydration kinetics of gypsum pastes prepared with a higher 1:1 water/solid ratio and cured at 100 % RH to favor hydration (complemented with *ex situ* XRD analysis of samples subjected to long term hydration) provided further insight into the effect of calcination *T* on the reactivity of bassanite and anhydrite II (Fig. 5b). This analysis revealed an extremely fast hydration within 15–20 min of gypsum calcined at 200 °C, originally containing ~ 80 wt% bassanite, 5 wt% anhydrite II and 10 wt% uncalcined gypsum. In the case of gypsum calcined at 300–400 °C, originally containing 75–90 wt% anhydrite II, it took 3 and 6 days, respectively, to obtain complete hydration. Gypsum calcined at 500 and 600 °C did not hydrate completely even after curing at 100 % RH for 8 days and samples still contained > 40 and 70 wt% anhydrite II, respectively. Calcination at 700 °C rendered anhydrite even less reactive and only ~ 5 wt% had transformed into gypsum after 8 days. It took 40 days to achieve almost complete hydration (i.e., ~95 wt % gypsum content, not included in Fig. 5b). Finally, gypsum calcined at 800 °C did not hydrate at all after 8 days and reached ~ 50 % hydration after 2 months. These findings are in good agreement with results by Schmid et al. [24], who also detected a drastic decrease in reactivity of gypsum calcined at $T \geq 650$ using Raman spectroscopy.

Considering the above results and to evaluate the possible effect of either uncalcined gypsum or newly formed anhydrite II on the kinetics of bassanite hydration, additional experiments comparing the hydration of paste samples prepared with pure bassanite and bassanite with varying amounts of uncalcined gypsum or insoluble anhydrite II were performed. These tests revealed that small gypsum or anhydrite II additions (i.e., 1, 5, 10, and 20 wt%) accelerated the setting of gypsum pastes significantly. Indeed, the hydration of bassanite was 2.4–3.2 times faster in the presence of 1–20 wt% gypsum, and no important differences regarding the influence of the varying amounts of gypsum were detected, suggesting that the threshold concentration for such acceleration was ≤ 1 wt% gypsum (Fig. 5c). In the case of anhydrite an acceleration was also observed (Fig. 5d), which, however, seemed to depend on the anhydrite concentration and was faster in pastes with 20 wt% anhydrite (i.e., bassanite hydration was 3.2 times faster than in pastes prepared with pure bassanite) as compared to samples containing only 1–10 wt% anhydrite (i.e., bassanite hydration was 1.6–2.0 times faster than in pastes prepared with pure bassanite). Apparently, the added gypsum and anhydrite II acted as seeds fostering heterogeneous nucleation. Gypsum seeds are known to promote homoepitaxial growth of gypsum crystals, whereas anhydrite II seeds can induce epitaxial growth of gypsum crystals [39], both effects leading to a reduction in the crystallization induction time [40,41]. Seeded crystallization has been employed in various technical processes including water desalination [42] and cement setting (i.e., addition of CSH seeds to accelerate setting) [43] but might be of limited use in the case of gypsum as slow-setting plasters are generally preferred for most applications.

These results suggest that hydration setting of multiphase gypsum will not only be influenced by the delayed anhydrite II hydration, but will also depend on the rate of bassanite hydration upon seeded crystallization in the presence of either anhydrite II or uncalcined gypsum. The fact that even small amounts (1 wt%) of either phase effectively accelerated hydration is of practical importance, suggesting that pure bassanite would be preferable for application that require sufficiently long setting times. The addition of an adequate amount (< 50 wt%) of anhydrite II could, however, be beneficial in applications where early strength or improved surface hardness are required (see section 3.3.). Uncalcined gypsum addition, in contrast, drastically reduces workability as it results in extremely fast hydration setting and does not seem recommendable for general use.

FESEM analysis showed that gypsum calcined at 100 °C underwent little changes upon hydration and only a few newly formed small gypsum crystals (arrows Fig. 6a) could be detected. This is consistent with XRD results (Fig. 3a), revealing that this sample contained ~ 95 wt% uncalcined gypsum. Plasters prepared with gypsum calcined at 200 °C

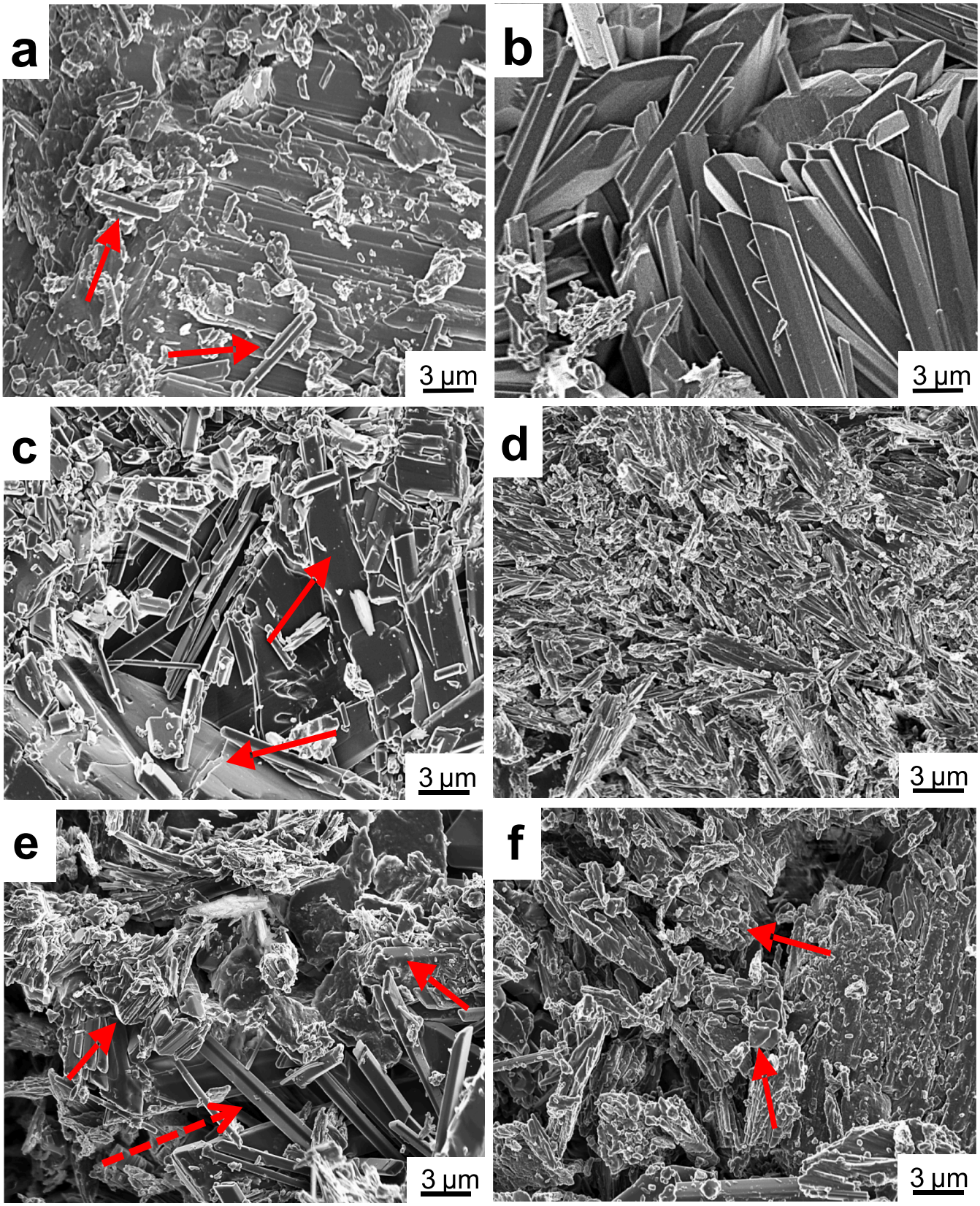

Fig. 6. FESEM images of calcined gypsum upon hydration: a) gypsum calcined at 100 °C, showing delamination along primary cleavage planes {0 1 0} of (partially) uncalcined gypsum and a few small newly formed gypsum crystals (arrows); b) gypsum calcined at 200 °C, showing newly formed large gypsum crystals with the typical acicular/blade-like habit together with c) grains of uncalcined gypsum (arrows); d) gypsum calcined at 400 °C, showing feather-like morphology of anhydrite; e) same sample, showing the partial disintegration of aggregated anhydrite crystals (arrows) together with acicular gypsum crystals (dashed arrow); and f) gypsum calcined at 800 °C showing partial disintegration of aggregated anhydrite crystals, some with rounded edges (arrows).

showed a continuous matrix formed by randomly oriented, interlocked gypsum crystals of up to 20 μm in size with the typical acicular/blade-like habit (Fig. 6b), which suffered, however, local disruption by larger uncalcined gypsum grains with plate-like morphology amounting to ~ 10 wt% (arrows, Fig. 6c). Newly formed gypsum crystals in the vicinity of uncalcined gypsum were smaller, with a maximum length of ~ 10 μm. Apparently, the seeded crystallization induced by the presence of uncalcined gypsum led to an increase in the nucleation rate and a decrease in crystal size [44]. Only partial hydration was obtained in plasters prepared with gypsum calcined at 300–400 °C, and large portions still maintained the feather-like morphology of anhydrite II (Fig. 6d). However, upon contact with water the larger aggregates of anhydrite II seemed to have disintegrated; now forming smaller clusters (arrows, Fig. 6e) together with acicular gypsum crystals with a maximum length of ~ 10 μm (dashed arrow, Fig. 6e). Gypsum calcined at 800 °C did not undergo any hydration, but a disintegration of the larger chunks of anhydrite II upon contact with water was observed. Some anhydrite II particles displayed rounded edges due to sintering (arrows, Fig. 6f).

Porosity and pore size distribution showed a clear relation with the plasteŕs mineralogical composition (Table 1). Plasters prepared with gypsum calcined at 200–250 °C (containing ~ 90–95 wt% hydrated gypsum) had an unimodal pore size distribution and ~ 15–20 % lower porosity as compared with samples prepared with gypsum calcined at 300–400 °C. Higher porosity in the case of the latter can be explained with the presence of large amounts of anhydrite II (40–70 wt%). As anhydrite II hydration involves a significant volume increase contributing to an overall decrease in porosity, it seems reasonable that plasters with untransformed anhydrite II displayed higher total porosity. The presence of large amounts of anyhydrite II also resulted in changes of the pore size distribution (Table 1, Fig. S2, Supplementary Material), being bimodal with a significant contribution of small pores with 0.01–0.5 μm diameter due to the presence of highly porous feather-like anhydrite II aggregates (Fig. 6d). In these samples, the portion of small pores was much larger (i.e., 32–37 % of the total porosity) as compared to plasters prepared with gypsum calcined at lower calcination T (≤250 °C) and only displaying needle-like gypsum crystals (i.e., only 6–10 % of the total porosity corresponds to pores with 0.01–0.5 μm diameter, Fig. 6b and Fig. S2, Supplementary Material). Microstructural changes caused by the presence of anhydrite II will have an important impact on the plasteŕs hygric/hydric behavior and weathering resistance as many studies have shown that an increase in pores with a diameter < 0.5 μm slows drying and leads to a decrease in salt weathering resistance [45,46]. However, considering the typically high porosity of historic plasters (i.e., 43–60 % porosity [13,47]), bassanite – anhydrite II mixtures could be useful for the design of compatible restoration materials with adequate porosity.

3.3. Strength and surface hardness of plasters

Significant differences in compressive/flexural strength and surface hardness (Leeb hardness) were detected in plasters prepared with gypsum calcined at different T (Fig. 7). All plasters fulfilled the requirements regarding compressive strength according to EN 13279–1 [27], but only the plaster prepared with gypsum calcined at 250 °C was above the minimum limit for flexural strength (i.e., minimum requirements for compressive and flexural strength being ≥ 2 and ≥ 1 MPa, respectively [27]). Generally, a direct relationship between porosity and mechanical strength is assumed [48]. However, here such relation could not be established (Table 1) and the mineralogical composition seemed to have been the decisive factor. Plaster prepared with gypsum calcined at 250 °C (containing ~ 95 wt% bassanite and ~ 5 wt% anhydrite) underwent almost complete hydration and developed a continuous matrix of interlocked acicular gypsum crystals, revealing the highest compressive and flexural strength. Remarkably, plaster prepared with gypsum calcined at 200 °C showed an almost 50 % decrease in strength as compared with the former plaster. It seems likely that the strength reduction was caused by the presence of ~ 10 wt% uncalcined gypsum in this sample, causing a local disruption of the plaster matrix as it does not act as a binder, but rather as a filler/aggregate without contributing to the formation of a strong and coherent matrix (Fig. 6c). Theoretically, the presence of ~ 10 wt% uncalcined gypsum produces an increase in the water/binder ratio from 0.6 to ~ 0.7 and gypsum will not undergo any hydration-related volume increase when in contact with water. As demonstrated here (see XRD results, above) the presence of uncalcined gypsum can also induce seeded crystallization and accelerate hydration setting. As a drawback, seeded crystallization can lead to the formation of gypsum aggregates lacking the interlocked acicular structure responsible for the strength of set gypsum. Indeed, changes in the morphology of gypsum (low aspect ratios) have been associated with a reduction in strength [44]. Karni and Karni [49] have studied the effect of variations in the water/solid ratio on compressive strength and observed a similar trend, which is generally explained with an increased pore volume at higher water/solid ratios, ultimately negatively influencing mechanical strength [7]. However, porosity measurements provided no evidence in this respect as samples prepared with gypsum calcined at 200 and 250 °C had almost identical porosity (Table 1). For plasters prepared with gypsum calcined at 300–400 °C, a clear relation between increasing anhydrite II content and strength decrease was detected. This was of no surprise as these plaster samples only contained between 30 and 55 wt% gypsum binder after curing, and according to SEM still displayed large chunks of unhydrated anhydrite II (40–70 wt%) (Fig. 5d and e). This finding is of great practical importance, as plaster with adequate strength might only be obtained after prolonged additional curing in order to achieve a sufficient degree of hydration. Indeed, the hydration kinetic study shows that complete hydration of anhydrite II might take months, depending on the calcination T and water availability (Fig. 5b). Based on these results, it seems reasonable to differentiate between the role played by anhydrite II obtained at 300–400 °C and that obtained at higher T. Anhydrite obtained at higher T, displayed higher crystallinity (Fig. 2b) and larger crystal size (Fig. 4d) and, as a result, lower reactivity (Fig. 5b), suggesting that it will not hydrate easily under ambient conditions and rather act as an aggregate. This is consistent with the presence of anhydrite II grains in many historic mortars and plasters [10,49]. In the case of anhydrite II obtained at 300–400 °C, only 20 % had hydrated after curing for 7 days and contributed to an interlocked plaster matrix. However, it is likely that the remaining anhydrite II will eventually hydrate under ambient conditions (Fig. 4b). Theoretically, delayed hydration of anhydrite II could result in a strength decrease. Vegas et al. [8] warns that delayed hydration of anhydrite II could lead to a disruption of the originally formed matrix of interlocked gypsum crystals and thus provoke a strength decrease, while Daritz et al. [32], Lenz and Sobott [50], and Sanz Arauz [51] advocate for an improvement in strength over time. The former is in line with previous observation regarding the negative effect of delayed ettringite formation on concrete performance [52]. However, it seems likely that additional cementation due to gypsum formation will cancel out the disruptive effect of delayed

Table 1
Porosity and pore size distribution of plasters prepared with gypsum calcined at different T.

Sample	Porosity (%)	Pore size distribution (Ø, μm)		Pores < 0.5 μm Ø (% of total porosity)
200 °C	38.0	unimodal	2.0	10
250 °C	39.0	unimodal	3.4	6
300 °C	42.6	bimodal	2.4/~ 0.1	37
350 °C	44.0	bimodal	2.6/~ 0.1	32
400 °C	46.7	bimodal	4.0/~ 0.1	34

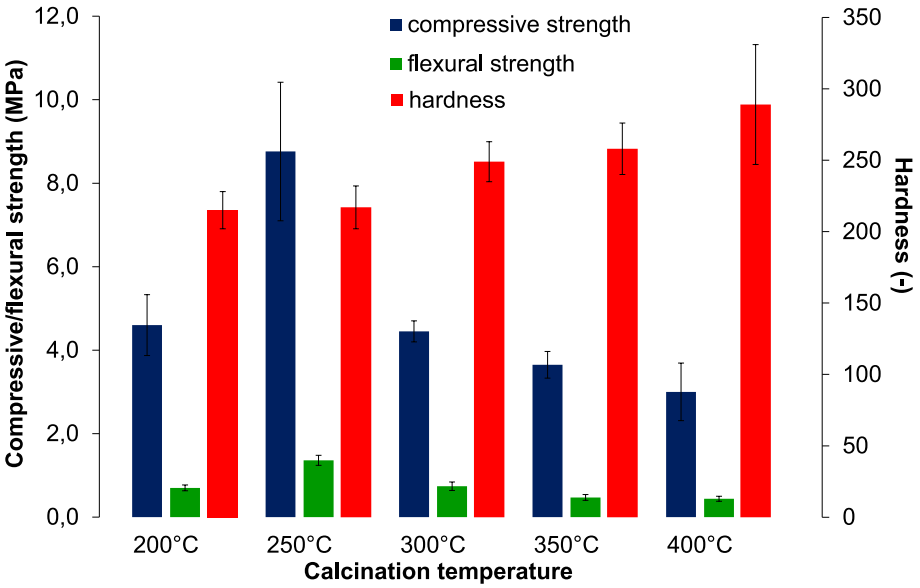

Fig. 7. Compressive/flexural strength and surface hardness of plasters prepared with gypsum calcined at various temperatures. Note that coherent plaster samples could not be obtained with gypsum calcined at < 200 °C and > 400 °C.

anhydrite II hydration and could lead to a densification of the plaster matrix. Considering the commonly low strength reported for historic gypsum-based plasters (i.e., 1.1–4.3 MPa compressive strength [47,53,54]), gypsum-anhydrite II mixtures could be used to prepare restoration materials, which fulfill the established compatibility requirements and have similar or lower strength than the original plasters [47,55].

Surface hardness (Fig. 7) did not follow the same trend and an increase was observed, which was proportional to the anhydrite II content in plasters prepared with gypsum calcined at 300–400 °C. Cured plasters containing 40–70 wt% anhydrite showed a 15–35 % increase in surface hardness as compared to cured plasters only containing gypsum. Additional experiments involving plasters with 0.6 water/solid ratio, containing either pure bassanite or 50 wt% bassanite and 50 wt% uncalcined gypsum or anhydrite II calcined at 800 °C, provided further insight into the effect of different calcium sulfate minerals on surface hardness. Remarkably, both additions had a positive effect on surface hardness (Table 2), which was ~ 35 % higher than that of plasters prepared with pure bassanite. Similar results have been reported by del Rio Merino et al. [56], who observed a 10–25 % increase in hardness of gypsum plasters upon addition of 25–50 wt% ceramic waste, which acted as an inert filler. According to XRD results, neither uncalcined gypsum nor anhydrite II underwent any significant mineralogical changes upon hydration. XRD analysis revealed a significantly higher $020/\overline{1}$ 21 gypsum Bragg peak intensity ratio in fully set plaster prepared with 50 wt% uncalcined gypsum (mixed with 50 wt% bassanite) as compared to the remaining plaster samples (Table 2). The higher ratio is indicative of an overdevelopment of (0 1 0) gypsum crystal faces due to crystals with plate-like morphology (Fig. S2). It seems that a sufficient amount of uncalcined gypsum with plate-like morphology is required to improve surface hardness, as no such effect was observed in plaster samples prepared with gypsum calcined at 200 °C containing only 10 wt % uncalcined gypsum, which is consistent with the lower $020/\overline{1}$ 21 gypsum Bragg peak intensity ratio calculated for this plaster (Table 2). In conclusion, a large amount of gypsum particles with plate-like morphology (indicated by a higher $020/\overline{1}$ 21 gypsum Bragg peak intensity ratio) seem to be responsible for the observed greater surface hardness in plaster with high uncalcined gypsum content. However, the plate-like particles might not necessarily contribute to a more interlocked matrix and thus do not improve compressive and flexural strength. In the case of anhydrite II-rich plasters, all samples containing ≥ 40 wt% anhydrite II consistently showed higher surface hardness than plasters prepared with pure bassanite (Table 2), which was likely related with the higher Mohs hardness of anhydrite (Mohs hardness = 3–3.5) as compared to that of gypsum (Mohs hardness = 2).

Table 2
$020/\overline{1}$ 21 gypsum Bragg peak intensity ratio and surface hardness of cured plasters (The $020/\overline{1}$ 21 gypsum Bragg peak intensity ratio of uncalcined gypsum is included for comparison).

Sample	$020/\overline{1}$ 21 Gypsum Bragg peak intensity ratio	Surface Hardness
Uncalcined gypsum	3.1 – 7.2	n.a.*
Plaster 200 °C**	1.1	215 ± 13
Plaster 250 °C**	1.0	217 ± 15
Plaster 300 °C**	1.0	249 ± 14
Plaster 350 °C**	1.0	258 ± 18
Plaster 400 °C**	1.1	289 ± 42
Plaster 100 wt% bassanite***	0.9	207 ± 8
Plaster 50 wt% bassanite + 50 wt % anhydrite***	0.9	278 ± 17
Plaster 50 wt% bassanite + 50 wt % gypsum***	1.4	286 ± 14

*not available.
**plasters prepared with gypsum calcined at different *T*.
***plasters prepared with 100 wt% bassanite or 50 wt% bassanite + 50 wt% anhydrite/gypsum.

3.4. Weathering resistance of plasters

The accelerated weathering test revealed significant differences in the resistance to degradation of the various plaster samples (Figs. 8 and 9). Plaster prepared with gypsum calcined at 250 °C showed the highest resistance against the impact of water spraying based on total weight loss. This sample contained ~ 95 wt% bassanite and 5 wt% anhydrite upon calcination, which hydrated readily and formed a continuous matrix of interlocked gypsum crystals according to XRD and FESEM analyses. Remarkably, plaster prepared with gypsum calcined at 300 °C showed almost identical weathering resistance, even though, the cured sample contained ~ 40 wt% anhydrite II, which did not contribute to the formation of a continuous matrix of interlocked gypsum crystals. The relatively good weathering resistance of this plaster might be explained by the lower dissolution rate of anhydrite as compared to gypsum, which

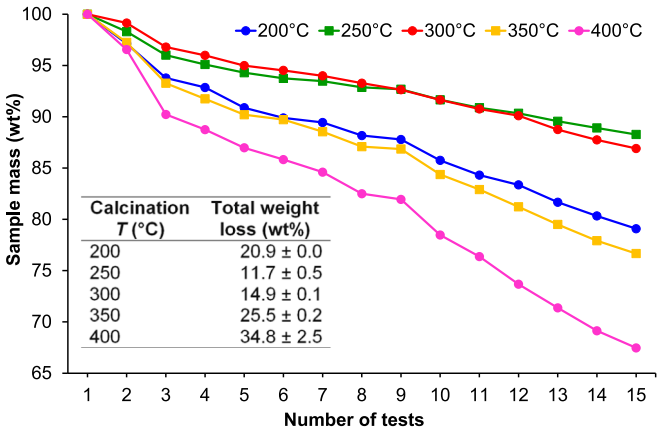

Fig. 8. Weight loss (wt%, corrected for weight gain due to hydration of calcium sulfate phases) upon water spraying of plaster samples prepared with gypsum calcined at different T (lines are a guide to the eye).

could have compensated for the lower effective binder content [57]. However, improved hardness due to the presence of anhydrite II could also have contributed to better resistance against the mechanical impact of water spraying. Plasters prepared with gypsum calcined at 350 and 400 °C revealed significantly lower weathering resistance, suggesting that a certain threshold regarding the permissible anhydrite II content cannot be surpassed. Likely, the large amount of untransformed anhydrite II (65–70 wt%) and the consequently low binder content (i.e., these plasters only contained 30–35 wt% of newly formed gypsum) were responsible for the decrease in weathering resistance. However, XRD analysis revealed that plaster samples originally containing 65–75 wt% anhydrite II reached complete hydration upon weathering (water spraying). These findings suggest that the weathering resistance of plasters prepared with gypsum calcined at $T \geq 300$ °C could probably be improved by prolonging the curing process (e.g., the plaster surface could be covered by plastic film to avoid premature drying) in order to achieve a higher degree of hydration and consequently higher binder content.

A clear relation between the plasters total porosity and their weathering resistance could not be established (Table 1). Despite the almost identical total porosity displayed by samples prepared with gypsum calcined at 200 and 250 °C, the former suffered a 70 % higher material loss over the course of the weathering test (Fig. 8). It is unknown whether the ~ 10 wt% uncalcined gypsum content in the former samples and the above-mentioned seeding effect was responsible for the lower resistance due to modifications in the microstructure [34]. More detailed studies are required to get a better insight into the influence of crystal morphology and microstructure on the plasters weathering resistance.

4. Conclusions

The outcome of this study revealed that under calcination conditions typically encountered in traditional kilns, it can be expected that uncalcined gypsum is the predominant phase in material calcined at $T \leq 150$ °C, while at 200–250 °C the material will contain mainly bassanite. Calcination at ≥ 300 °C will result in high (≥75 wt%) anhydrite II content and at 500 °C, anhydrite II will be the only phase. Crystallite size measurements (based on XRD analysis) proved useful to assess the sintering degree of anhydrite II. Anhydrite II calcined at ≥ 600 °C, displayed pronounced sintering as confirmed by SEM and, consequently, extremely low reactivity as demonstrated by hydration kinetics studies, which showed that after 2 months only 50 % hydration was achieved in material calcined at 800 °C. As a result, coherent plaster samples could only be obtained with gypsum calcined between 200 and 400 °C, which contained sufficient bassanite to produce a continuous matrix upon hydration under ambient conditions.

Hydration kinetics studies also demonstrated that anhydrite II and especially uncalcined gypsum additions accelerated bassanite hydration likely by fostering seeded crystallization. This could be beneficial as it induces fast setting but seems to have an adverse effect on final strength. The presence of both phases should be avoided if slow setting is required.

Delayed anhydrite II hydration was the cause of low strength and weathering resistance in plasters prepared with gypsum calcined at $T \geq 300$ °C, but could, at least in part, be prevented by prolonging the curing process (i.e., avoiding premature drying of plasters) in order to facilitate the formation of gypsum binder. The only partial hydration of anhydrite in these plasters leads to an increase in the water/binder ratio, because the unhydrated anhydrite II acts as aggregate. Historic evidence indicates that experienced masons often adjusted the pastés water content in the case of high-fired gypsum in order to obtain a dense and resistant plaster, which might even improve over time due to continuous dissolution-crystallization processes, leading to additional gypsum formation and causing a reduction in porosity.

Remarkably, higher surface hardness was observed in the presence of large amounts of anhydrite II and uncalcined gypsum. This was surprising, as small amounts of larger plate-like uncalcined gypsum grains seemed to cause a disruption of the continuous gypsum crystal matrix and had a negative effect on strength and weathering resistance. Likely morphological changes (i.e., presence of more plate-like gypsum crystals with higher 020/$\bar{1}$ 21 Bragg peak ratio) induced by the presence of uncalcined gypsum were responsible for improved surface hardness, but did not contribute to a more interlocked plaster matrix, essential for higher compressive and flexural strength and weathering resistance. In the case of anhydrite II, improved surface hardness was probably related with its higher Mohs hardness (3–3.5) as compared to that of gypsum (2).

Additional studies should be performed in order to evaluate the effect of delayed anhydrite II hydration with regard to possible volume changes (i.e., considering the molar volume of anhydrite and gypsum, hydration of anhydrite II could either lead to deleterious expansion or

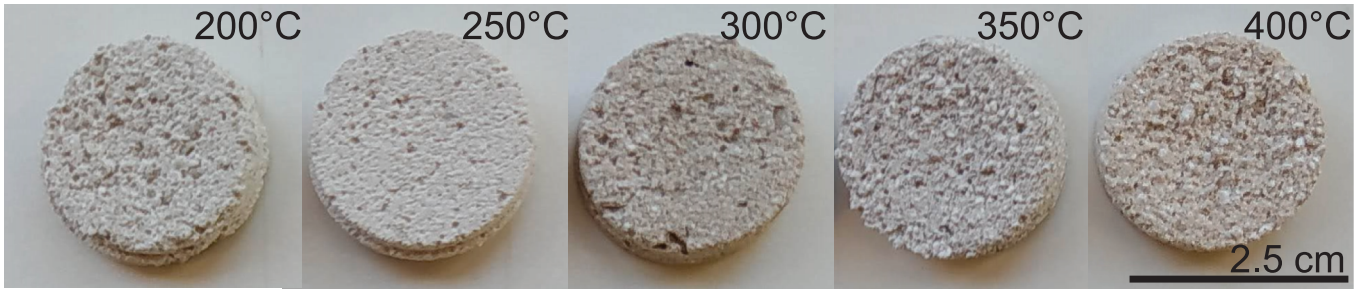

Fig. 9. Aspect of plaster samples prepared with gypsum calcined at different T after the completion of the weathering test, showing different degrees of material loss.

beneficial densification) in set gypsum plasters and how these changes will affect strength and weathering resistance over time. The research on artificial calcium sulfate phase mixtures should be extended to get a better understanding regarding the effect of uncalcined gypsum and anhydrite II additions on gypsum crystal morphology and the micro-textural development in set plasters. To this end, additional analytical techniques such as confocal microscopy and contact angle measurements could be applied to get a better insight into the plasters surface properties, including roughness and wettability. Systematic studies of artificial calcium sulfate phase mixtures would also be useful in order to determine the threshold for certain individual phases (i.e., uncalcined gypsum and unreactive anhydrite II calcined at different *T*) and design optimized mixtures for specific applications, including compatible restoration materials with suitable porosity and mechanical strength, and improved weathering resistance.

Funding

This research was financed by the Unidad de Excelencia "UCE2018-01 - Ciencia en la Alhambra" (Universidad de Granada, UGR), Unidad Cientifica de Excelencia "UCE.PP2016.05" (UGR), the Master "Ciencias y Tecnologia en Patrimonio Arquitectónico" (UGR), the Research Group "RNM0179" (Junta de Andalucia), and the Spanish government (grant RTI2018-099565-B-I00). MBR is recipient of a grant (PRE2019-090256) by the Spanish Government. Funding for open access charge: Universidad de Granada / CBUA

CRediT authorship contribution statement

Kerstin Elert: Conceptualization, Methodology, Investigation, Writing – original draft, Writing – review & editing, Visualization. **Pedro Bel-Anzué:** Conceptualization, Investigation, Writing – review & editing. **Miguel Burgos-Ruiz:** Investigation, Writing – review & editing.

Declaration of Competing Interest

The authors declare that they have no known competing financial interests or personal relationships that could have appeared to influence the work reported in this paper.

Data availability

Data will be made available on request.

Acknowledgement

We thank Dr. C. Rodriguez-Navarro for insightful comments and suggestions.

Appendix A. Supplementary data

Supplementary data to this article can be found online at https://doi.org/10.1016/j.conbuildmat.2023.130361.

References

[1] W.D. Kingery, P. Vandiver, M. Prickett, The beginnings of pyrotechnology, part II: production and use of lime and gypsum plaster in the Pre-Pottery Neolithic Near East, J. Field. Archaeol. 15 (1988) 219–224.
[2] P. Bel-Anzué, K. Elert, Changes in traditional building materials: the case of gypsum in Northern Spain, Archaeol. Anthropol. Sci. 13 (2021) 117.
[3] D. Sanz Arauz, A. Sepulcre Aguilar (Eds.), El Yeso En La Arquitectura Histórica, UPM Press, Madrid, 2022.
[4] B. Middendorf, Physico-mechanical and microstructural characteristics of historic and restoration mortars based on gypsum: current knowledge and perspective, Geological Society, London, Special Publications 205 (1) (2002) 165–176.
[5] V. La Spina, C.J. Grau Giménez, La diversidad tipológica de los hornos tradicionales de calcinación de yeso en España, Inf. de la Construcción 72 (557) (2020) 334.
[6] M.T. Freire, A. Santos Silva, M.d.R. Veiga, J.d. Brito, Studies in ancient gypsum based plasters towards their repair: Mineralogy and microstructure, Construct, Build. Mater. 196 (2019) 512–529.
[7] N. Lushnikova, L. Dvorkin, Sustainability of gypsum products as a construction material, in: J.M. Khatib (Ed.), Sustainability of Construction Materials, Woodhead Publishing Series in Civil and Structural Engineering: Number 17, Elsevier, Amsterdam, 2016, pp. 643–681.
[8] F. Vegas, C. Mileto, F. Fratini, S. Rescic, May a building stand upon gypsum structural walls and pillars? The use of masonry made of gypsum in traditional architecture in Spain, in: W. Jäger, B. Haseltine, A. Fried (Eds.), Proceedings of the 8th International Masonry Conference, International Masonry Society and Technische Universität Dresden, 4.-7. July 2010, pp. 2183–2219.
[9] R. Lenz, Die Wiederentdeckung einer verlorenen Materialkultur: Hochbrand-Gipsböden in Sachsen-Anhalt zwischen Konservierung, Restaurierung und Rekonstruktion, in: G. Biscontin, G. Drussi (Eds.), Pavimentazioni storiche: uso e conservazione, XXII Convegno Scienza e Beni Culturali di Bressanone (Brixen), 11.-14. July 2006, pp. 355-361.
[10] T. Kawiak, Gypsum mortars from a twelfth-century church in Wiślica, Poland, Stud. Conserv. 36 (1991) 142–150.
[11] T. Schmid, R. Jungnickel, P. Dariz, Raman band widths of anhydrite II reveal the burning history of high-fired medieval gypsum mortars, J. Raman Spectrosc. 50 (8) (2019) 1154–1168.
[12] M.T. Freire, A. Santos Silva, M. do Rosário Veiga, C.B. Dias, A. Manhita, Stucco marble in the Portuguese architecture: multi-analytical characterization, Int. J. Archit. Herit. 14 (2020) 977–993.
[13] F.J. Blasco-López, F.J. Alejandre Sánchez, Porosity and surface hardness as indicators of the state of conservation of Mudéjar plasterwork in the Real Alcázar in Seville, J. Cult. Herit. 14 (2) (2013) 169–173.
[14] X. Li, Q. Zhang, Dehydration behaviour and impurity change of phosphogypsum during calcination, Constr. Build. Mater. 311 (2021), 125328.
[15] J. Hao, G. Cheng, T. Hu, B. Guo, X. Li, Preparation of high-performance building gypsum by calcining FGD gypsum adding CaO as crystal modifier, Constr. Build. Mater. 306 (2021), 124910.
[16] M.A. Pedreno-Rojas, I. Flores-Colen, J. De Brito, C. Rodríguez-Linán, Influence of the heating process on the use of gypsum wastes in plasters: Mechanical, thermal and environmental analysis, J. Clean. Prod. 215 (2019) 444–457.
[17] A. Koper, K. Prałat, J. Ciemnicka, K. Buczkowska, Influence of the calcination temperature of synthetic gypsum on the particle size distribution and setting time of modified building materials, Energies 13 (2020) 5759.
[18] G. Camarini, K.D. dos Santos Lima, S.M.M. Pinheiro, Investigation on gypsum plaster waste recycling: an eco-friendly material, Green Mater. 3 (4) (2015) 104–112.
[19] W. Cao, W. Yi, J. Peng, J. Li, S. Yin, Recycling of phosphogypsum to prepare gypsum plaster: effect of calcination temperature, J. Build. Eng. 45 (2022), 103511.
[20] J. Jiao, X. Shen, H. Ding, D. Lu, D. Li, Study on the hydration and properties of multiphase phosphogypsum synergistically activated by sodium sulfate and calcium sulfate whisker, Constr. Build. Mater. 355 (2022), 129225.
[21] R.H. Geraldo, S.M. Pinheiro, J.S. Silva, H.M. Andrade, J. Dweck, J.P. Gonçalves, G. Camarini, Gypsum plaster waste recycling: A potential environmental and industrial solution, J. Clean. Prod. 164 (2017) 288–300.
[22] J.D. Martin, Using XPowder: a software package for Powder X-Ray difraction analysis (GR, 1001/04, ISBN 84–609–1497–6), 2004.
[23] S. Seufert, C. Hesse, F. Goetz-Neunhoeffer, J. Neubauer, Quantitative determination of anhydrite III from dehydrated gypsum by XRD, Cem. Concr. Res. 39 (10) (2009) 936–941.
[24] T. Schmid, R. Jungnickel, P. Dariz, Insights into the $CaSO_4$–H_2O system: A Raman-spectroscopic study, Minerals 10 (2020) 115.
[25] A.E. Charola, S.A. Centeno, Analysis of gypsum-containing lime mortars: possible errors due to the use of different drying conditions, J. Am. Inst. Conserv. 41 (2002) 269–278.
[26] European committee for standardization EN 1015–11, Methods of test for mortar for masonry - Part 11: Determination of flexural and compressive strength of hardened mortar 2019 Brussels.
[27] European committee for standardization EN 13279–1, Gypsum binders and gypsum plasters - Part 1: Definitions and requirements 2008 Brussels.
[28] Y. Deutsch, Y. Nathan, S. Sarig, Thermogravimetric evaluation of the kinetics of the gypsum-hemihydrate-soluble anhydrite transitions, J. Therm. Anal. 42 (1) (1994) 159–174.
[29] C. Pritzel T. Kowald Y. Sakalli R. Trettin Binding materials based on calcium sulphates: Composition, Properties, Application (Chap. 9) H.H. Pöllmann Cementitious materials: Composition, properties, application 2017 de Gruyter Berlin.
[30] O. Chaix-Pluchery, J. Pannetier, J. Bouillot, J.C. Niepce, Structural prereactional transformations in $Ca(OH)_2$, J. Solid State Chem. 67 (2) (1987) 225–234.
[31] A. Nørlund Christensen, M. Olesen, Y. Cerenius, T.R. Jensen, Formation and transformation of five different phases in the CaSO4− H2O system: crystal structure of the subhydrate β-$CaSO_4$·0.5 H_2O and soluble anhydrite $CaSO_4$, Chem. Mater. 20 (2008) 2124–2132.
[32] P. Dariz, C. Jakob, D. Ectors, J. Neubauer, T. Schmid, Measuring the burning temperatures of anhydrite micrograins in a high-fired Medieval gypsum mortar, Chem. Select 2 (2017) 9153–9156.
[33] A.K. Galwey, M.E. Brown, Thermal decomposition of ionic solids: chemical properties and reactivities of ionic crystalline phases, Elsevier, Amsterdam, 1999.

[34] D. Aquilano, F. Otálora, L. Pastero, J.M. García-Ruiz, Three study cases of growth morphology in minerals: Halite, calcite and gypsum, Prog. Cryst. Growth Charact. Mater. 62 (2) (2016) 227–251.
[35] I.J.A. Carreño-Marquez, E. Menéndez-Méndez, H.E. Esparza-Ponce, L. Fuentes-Cobas, R. García-Rovés, I. Castillo-Sandoval, M. Luna-Porres, J. de-Frutos-Vaquerizo, M.E. Montero-Cabrera, Naica's giant crystals: deterioration scenarios, Cryst. Growth Design 18 (8) (2018) 4611–4620.
[36] W. Abriel, K. Reisdorf, J. Pannetier, Dehydration reactions of gypsum: A neutron and X-ray diffraction study, J. Solid State Chem. 85 (1990) 23–30.
[37] C. Rodríguez-Navarro, Binders in historical buildings: Traditional lime in conservation, Semin. SEM 9 (2012) 91–112.
[38] F. Hernández-Olivares, V. Aguado, E. Menéndez, L. de Villanueva, Sintering of natural anhydrite-glass composite, J. Eur. Ceram. Soc. 17 (5) (1997) 743–748.
[39] C. Pina, U. Becker, L. Fernández-Díaz, Crecimiento epitaxial de yeso sobre anhidrita: Estudio in situ mediante microscopía de fuerza atómica (AFM), CAD. LAB. XEOL. LAXE 25 (2000) 31-33.
[40] J.Y. Choi, T. Lee, Y. Cheng, Y. Cohen, Observed crystallization induction time in seeded gypsum crystallization, Ind. Eng. Chem. Res. 58 (51) (2019) 23359–23365.
[41] H.B. Weiser, F.B. Moreland, The setting of plaster of Paris, J. Phys. Chem. 36 (1) (1932) 1–30.
[42] P. Sanciolo, E. Ostarcevic, P. Atherton, G. Leslie, T. Fane, Y. Cohen, M. Payne, S. Gray, Enhancement of reverse osmosis water recovery using interstage calcium precipitation, Desalination 295 (2012) 43–52.
[43] H.C. Pedrosa, O. Mendoza Reales, V. Dias Reis, M. das Dores Paiva, E. Moraes Rego Fairbairn, Hydration of Portland cement accelerated by CSH seeds at different temperatures, Cem. Concr. Res. 129 (2020), 105978.
[44] A.J. Lewry, J. Williamson, The setting of gypsum plaster. Part III The effect of additives and impurities, J. Mater. Sci. 29 (23) (1994) 6085–6090.
[45] G.W. Scherer, Theory of drying, J. Am. Ceram. Soc. 73 (1) (1990) 3–14.
[46] C. Rodriguez-Navarro, E. Doehne, Salt weathering: influence of evaporation rate, supersaturation and crystallization pattern, *Earth Surf. Process.* Landf. 24 (1999) 191–209.
[47] M.T. Freire, M. do Rosário Veiga, A.S. Silva, J. de Brito, Studies in ancient gypsum based plasters towards their repair: Physical and mechanical properties, Constr. Build. Mater. 202 (2019) 319–331.
[48] D. Liu, B. Šavija, G.E. Smith, P.E.J. Flewitt, T. Lowe, E. Schlangen, Towards understanding the influence of porosity on mechanical and fracture behaviour of quasi-brittle materials: experiments and modeling, Int. J. Fract. 205 (2017) 57–72.
[49] J. Karni, E. Karni, Gypsum in construction: origin and properties, Mater. Struct. 28 (2) (1995) 92–100.
[50] R. Lenz, R. Sobott, Beobachtungen zu Gefügen historischer Gipsmörtel, in: M. Auras, H.-.-W. Zier (Eds.), Gipsmörtel im historischen Mauerwerk und an Fassaden, WTA Publications, Munich, 2008, pp. 23–34.
[51] D. Sanz Arauz, Análisis del yeso empleado en revestimientos exteriores mediante técnicas geológicas, Universidad Politécnica, Madrid, 2009. PhD Thesis.
[52] M. Collepardi, A state-of-the-art review on delayed ettringite attack on concrete, Cem. Conc. Comp. 25 (4-5) (2003) 401–407.
[53] A. Al-Sibahy, R. Edwards, Structural evaluation for the historic Palace of King Ghazi and mechanism of its rehabilitation, Case Stud. Constr. Mater. 13 (2020) e00371.
[54] T. Freire, A.S. Silva, R. Veiga, J. De Brito, Characterization of Portuguese historical gypsum mortars: a comparison between two case studies, Mater. Sci. Forum 636 (2010) 1258–1265.
[55] J. De Brito I. Flores-Colen Renders M.C. Gonçalves F. Margarido Materials for Construction and Civil Engineering 2015 Springer Cham 123 184.
[56] M. del Río Merino, J. Santa Cruz Astorqui, P. Villoria Sáez, R. Santos Jiménez, M. González Cortina, Eco plaster mortars with addition of waste for high hardness coatings, Constr. Build. Mater. 158 (2018) 649–656.
[57] A. Klimchouk, The dissolution and conversion of gypsum and anhydrite, Int. J. Speleol. 25 (1996) 21–36.